coatings

MDPI

Article

Multi-Walled Carbon Nanotube-Assisted Electrodeposition of Silver Dendrite Coating as a Catalytic Film

Li Fu [1,*], Kefeng Xie [2], Huaiwei Zhang [1], Yuhong Zheng [3], Weitao Su [1] and Zhong Liu [4,*]

1 Collage of Materials and Environmental Engineering, Hangzhou Dianzi University, Hangzhou 310018, China; zhw5984@hdu.edu.cn (H.Z.); suweitao@hdu.edu.cn (W.S.)
2 State Key Laboratory of Plateau Ecology and Agriculture, Qinghai University, Xining 810016, China; xiekf12@lzu.edu.cn
3 Institute of Botany, Jiangsu Province and Chinese Academy of Sciences, Nanjing Botanical Garden Mem. Sun Yat-Sen, Nanjing 210014, China; yuhongzhengcas@gmail.com
4 Key Laboratory of Comprehensive and Highly Efficient Utilization of Salt Resources, Qinghai Institute of Salt Lakes, Chinese Academy of Sciences, Xining 810008, China
* Correspondence: fuli@hdu.edu.cn (F.L.); liuzhong@isl.ac.cn (Z.L.); Tel.: +86-571-8272-8857 (F.L.); +86-971-6320-622 (Z.L.)

Academic Editors: Wei Gao and Yuxin Wang
Received: 17 November 2017; Accepted: 12 December 2017; Published: 14 December 2017

Abstract: A multi-walled carbon nanotube (MWCNT)-coated indium tin oxide (ITO) slide was used as a platform for the growth of a silver dendrite (Ag-D) film using cyclic voltammetry. The particular dendritic nanostructures were formed by the diffusion-limited-aggregation model due to the potential difference between the MWCNTs and the ITO surface. The Ag-D-coated ITO film was then used for the catalytic degradation of methyl orange (MO) and methylene blue (MB) under static aqueous conditions. The network structure of the Ag-D allows the efficient diffusion of MO and MB, and consequently enhances the catalytic performance. Since the thin film is much easier to use for the post-treatment of powder catalysts, the proposed method shows great potential in many catalytic applications.

Keywords: silver dendrites; multi-walled carbon nanotubes; catalytic degradation; electrodeposition

1. Introduction

Metal nanostructures have received considerable attention due to their advanced properties compared with their bulk form [1–3]. Many applications have been developed based on their superior properties, in areas such as biosensing, catalysis, thermal transportation, surface-enhanced Raman spectroscopy (SERS), and pollutant adsorption [4–12]. Among different nanostructures, the dendritic nanostructure has attracted considerable interest due to its unique morphology and properties [13–16]. The dendritic metal nanostructure consists of some major trunks with many hierarchical branches and leaves. This loose and connected network morphology offers a porous and stable structure, and shows excellent adsorption and diffusion abilities. Therefore, metal dendrites have potential applications in the areas of catalysis, SERS, and sensing, in particular [17–20].

Among metal dendrites, the silver dendrite (Ag-D) is much closer to being used in real applications than other metal dendrites because of its low cost and relatively facile synthesis [21–26]. For example, our previous work reported the synthesis of Ag-D based on a galvanic replacement method [27]. However, the use of a sacrificial metal (aluminum in our case) for Ag-D formation cannot avoid the contamination of counterpart ions. To overcome this problem, we proposed an electrochemical deposition method for the formation of an Ag-D coating with the assistance of multi-walled carbon

nanotubes (MWCNTs) and graphene oxide [28]. The high price of the graphene oxide still restricts its further application. In this work, we further propose a potentiostatic deposition method for Ag-D deposition on an indium tin oxide (ITO) slide, with assistance only from MWCNTs. The surface hydroxyl groups of the MWCNTs attracted the Ag^+ ions in the solution, and consequently formed crystal nuclei. Then, Ag-D were formed by a diffusion-limited-aggregation (DLA) model as a result of the local potential difference between the MWCNTs and the ITO substrate. The Ag-D-deposited ITO was then applied for the catalytic degradation of methylene blue (MB) and methyl orange (MO) dyes in the presence of $NaBH_4$.

2. Materials and Methods

Silver nitrate ($AgNO_3$), $NaBH_4$, methylene blue (MB) and methyl orange (MO) were purchased from Sigma (Melbourne, Australia). Multi-walled carbon nanotubes (purity $\geq$ 95%, length 1–2 μm) were purchased from Shenzhen Nanotech Port Co., Ltd. (Shenzhen, China). All other chemicals were analytical grade reagents. ITO-coated glasses (R_{est} = 10 $\pm$ 2 Ω) were purchased from Huanan Xiangcheng Tech. Co., Ltd. (Chenzhou, China).

Oxidation of MWCNT was carried out according to our previous work [29] with some modifications. Briefly, 10 mg MWCNT was oxidized in a 20 mL mixture of HNO_3 and H_2SO_4 (1:3, *v*/*v*) under sonication for 2 h. The resulting solution was filtered through a polyether sulfone filter paper (pore size of 200 nm) to remove the acids. The pH was washed using water till neutral. The oxidized MWCNTs were then collected and dried in an oven. The resultant can be easily dispersed into ethanol through a simple sonication, due to the formation of oxygen-containing groups on the wall surface.

For ITO surface coating, 0.5 mL of MWCNTs ethanol suspension (1 mg/mL) was spin-coated onto the ITO surfaces, and dried at room temperature (denoted as MWCNT/ITO). The potentiostatic electrodeposition of Ag-D was carried out using a CHI 832 electrochemical workstation (CH Instruments, Austin, TX, USA) at −1.4 V in 0.1 M HNO_3 with the presence of 0.1 mM $AgNO_3$. The deposition was carried out using a three-electrode system (reference electrode: Ag/AgCl (3 M KCl); auxiliary electrode: Pt wire). After electrodeposition, the Ag-D coated ITO was washed using water and ethanol. The resulting Ag-D-coated ITOs were denoted as Ag-D/ITO-1, Ag-D/ITO-2, and Ag-D/ITO-3, which had deposition times of 20 s, 40 s, and 60 s, respectively.

The morphology of Ag-D was characterized using a scanning electron microscope (SEM, ZEISS SUPRA 40VP, Carl Zeiss, Jena, Germany). The XRD patterns of the Ag-D samples were collected using an X-ray diffractometer (D2 Phaser, Bruker, Billerica, MA, USA) with Cu Kα radiation (λ = 1.5405 Å). The optical properties of the samples were obtained using UV-Vis spectrophotometer Lambda 35 (Perkin Elmer, Waltham, MA, USA).

For catalytic degradation of MB and MO, MWCNT/ITO or Ag-D/ITO slide was placed at the bottom of a Petri dish containing 20 mL of MB or MO aqueous solution (15 mg/L). Then, 0.5 mL of $NaBH_4$ (0.5 M) was injected into the Petri dish. The catalytic degradation process was monitored by UV-Vis spectroscopy at regular time intervals.

3. Results and Discussion

The morphologies of the Ag-Ds formed at different deposition times are shown in Figure 1. Figure 1A shows that the electrodeposition of Ag without the MWCNT coating resulted only in Ag clusters. Figure S1A shows that the potentiostatic treatment of MWNCTs without Ag precursor cannot affect the morphology of MWCNTs, while the dendrites formed only in the presence of $AgNO_3$ (Figure 1B–D). The electrodeposition time also plays an important role during Ag-D formation. As shown in Figure 1B, Ag-D/ITO-1 shows only the initiation of Ag-D on the MWCNT surface. After 60 s of deposition, distinct Ag-D was formed on the ITO surface with a porous network structure (Figure 1D). The formation of Ag-D with the assistance of MWCNTs can be explained as follows: the surface-hydroxylated MWCNTs were able to attract Ag^+ ions as a pre-absorption step. These Ag^+ ion-rich centers are first nucleated during the electrodeposition. Under an electric

field, the Ag nucleation normally prefers a spherical shape. However, the presence of the MWCNTs provides a potential difference between the ITO pre-formed Ag nucleus and the ITO surface. Therefore, Ag growth occurred under non-equilibrium growth conditions. The growth of the initial Ag-D was then controlled by a typical diffusion-limited-aggregation (DLA) [28,30,31]. The Ag^+ ions in the electrolyte then migrated to the tips of the initial Ag-D and resulted in continuous growth and elongation.

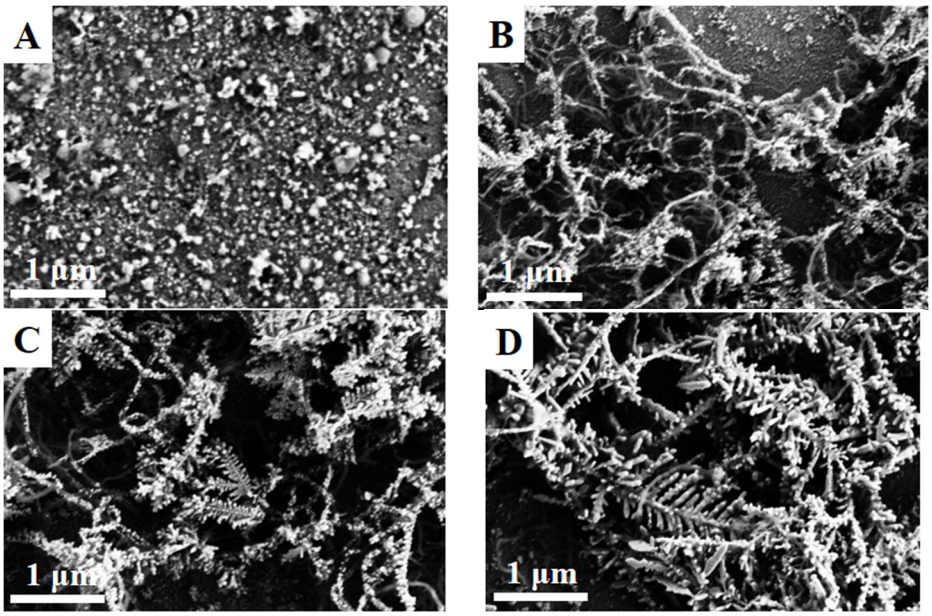

Figure 1. SEM images of (**A**) Ag deposition without MWCNTs, (**B**) Ag-D/ITO-1, (**C**) Ag-D/ITO-2 and (**D**) Ag-D/ITO-3.

The UV-Vis spectra of the Ag-D were recorded, and are shown in Figure 2A. The Ag-D were removed from the ITO surface through a 5-min sonication process, and then dispersed in water for characterization. As shown in Figure 2A, the spectrum of Ag-D-1 showed a characteristic absorption peak at 356 nm, which corresponds to the surface plasmon resonance (SPR) absorption [32]. Two similar spectra were recorded at Ag-D-2 and Ag-D-3. Noticeably, the characteristic peak for Ag-D showed a continuous widening along with deposition time. Since the SPR absorption of Ag is highly related to the size and structure of the nanostructure, the silver dendrites can be considered as the mixture of different-sized silver nanoparticles (branch, stem and leaf). Therefore, the broad peak with a long tail indicates the formation of Ag-D in a supramolecular structure [33–35]. The UV-Vis spectrum of the MWCNTs was also recorded, and is shown in Figure S1B. The spectrum shows a flat and smooth background feature without any distinct peak in the range of 300–600 nm. The spectrum also presented a typical absorption band at 260 nm, which can be attributed to the π–π^* transition characteristic of the MWCNTs.

The XRD patterns of the Ag-D were also collected to determine the crystal phase changes during the deposition. The samples for XRD analysis were also prepared using sample dispersion on a mica substrate. As shown in Figure 2B, XRD patterns of Ag-D-1, Ag-D-2 and Ag-D-3 all show distinct peaks at 35.44°, 42.71°, 62.46°, 75.67° and 79.66°, corresponding to the (111), (200), (220), (311) and (222) silver face-centered-cubic (fcc) crystal diffractions, respectively. However, the peak of (111) showed significant growth, suggesting the Ag-D growth prefers the (111) planes during the electrodeposition process. The XRD pattern of the MWCNTs exhibits the typical peaks at 25.6° and 42.7° (Figure S1C), corresponding to the graphite (002) and (100) reflections. These peaks were absent in the Ag-Ds, probably due to the surface silver coverage of the MWCNTs and the strong silver signals.

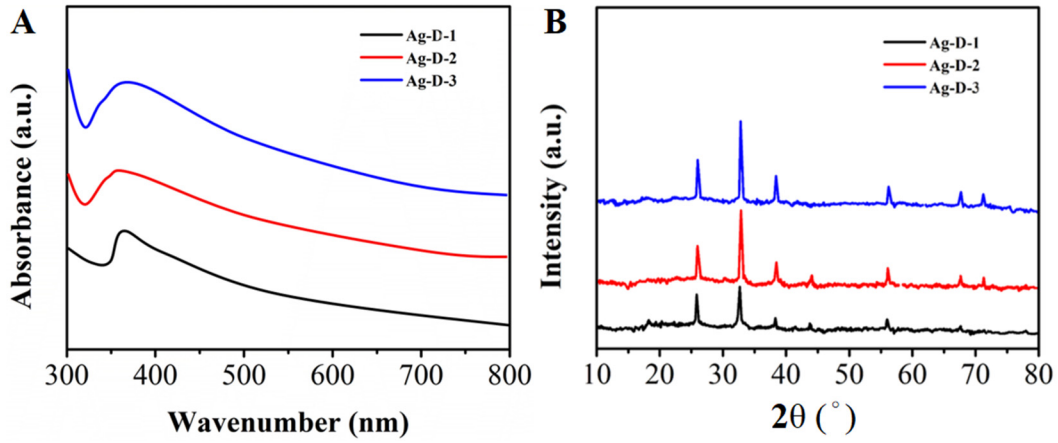

Figure 2. (**A**) UV-Vis spectra of Ag-D-1, Ag-D-2 and Ag-D-3; (**B**) XRD patterns of Ag-D/ITO-1, Ag-D/ITO-2 and Ag-D/ITO-3.

The catalytic activities of the Ag-D/ITO have been investigated using MO and MB in the presence of $NaBH_4$. The spectra recorded in the absence of catalyst does not show a clear dye-degradation reaction. Figure 3 shows the UV-Vis absorption spectra of the MO and MB with different catalysts after 30 min. It can be seen that the MO and MB solution showed slight decreases in absorbance in the presence of MWCNT/ITO, probably due to the adsorption effect. On the other hand, the presence of Ag-based catalysts showed significant decreases in the absorbance of both dyes, suggesting that silver nanostructures could catalyze the decomposition process by reducing the activation energy. Among the Ag-D/ITOs, Ag-D/ITO-3 showed more promising catalytic activity, compared with those of Ag-D/ITO-1 and Ag-D/ITO-2. We also conducted the catalytic reaction using Ag/ITO deposited without the assistance of MWCNTs (60 s deposition). It can be seen that the Ag/ITO showed a lower catalytic performance than Ag-D/ITO. Therefore, the porous dendritic structure of the Ag-D coating is more favorable than the normal Ag coating for catalysis. In addition, the presence of MWCNTs could efficiently adsorb dye molecules via the π–π stacking interaction, resulting in a high concentration of dye molecules around the Ag dendrites [27].

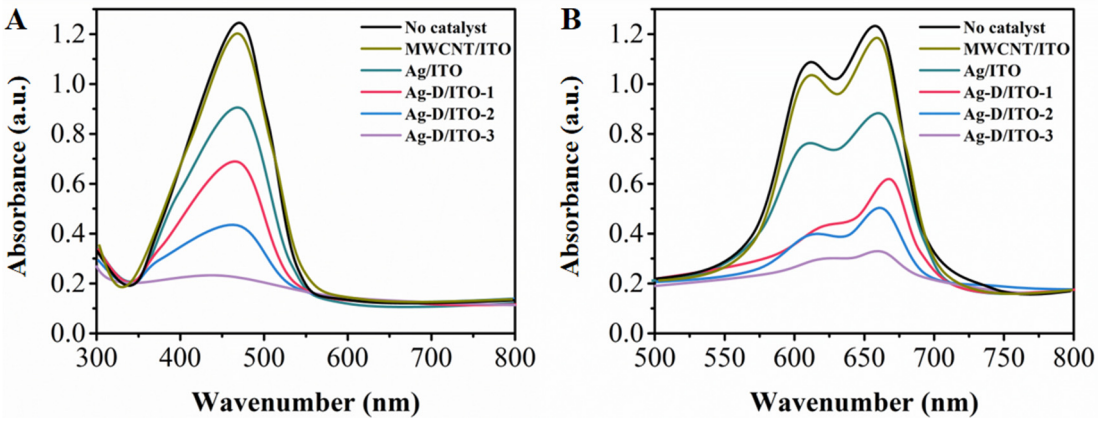

Figure 3. UV-Visible spectra of (**A**) MO and (**B**) MB degraded by MWCNT/ITO, Ag-D/ITO-1, Ag-D/ITO-2, Ag-D/ITO-3, Ag/ITO and without a catalyst after 30 min degradation.

Figure 4 shows the monitored degradation process of MO and MB in the presence of Ag-D/ITO-1, Ag-D/ITO-2 and Ag-D/ITO-3. Catalysis occurs only on the surface of metals; therefore, increasing the available surface area will greatly enhance the effectiveness of the catalyst [36,37]. From the figure, it can be observed that the catalytic degradation processes all exhibited a sharp increase in the initial

stage, since both the absorption and degradation occurred simultaneously. The following formula was used to represent the degradation performance:

$$\eta = \left(\frac{A_0 - A_t}{A_0} \right) \times 100\% \quad (1)$$

where A_0 is the initial absorbance of dyes solution and A_t is the absorbance of the dyes at time t [38]. The result indicates that all Ag-D/ITOs are able to fully degrade both dyes within 2 h. Among them, Ag-D/ITO-3 shows the highest degradation performance, in which more than 95% of both MO and MB were degraded within 60 min and 80 min, respectively.

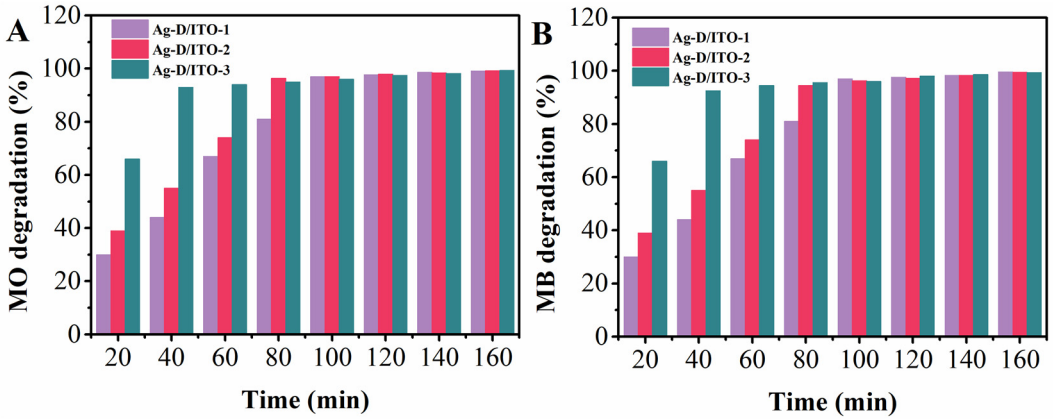

Figure 4. Catalytic degradation of (**A**) MO and (**B**) MB by $NaBH_4$ in the presence of Ag-D/ITO-1, Ag-D/ITO-2, Ag-D/ITO-3.

Pseudo-first-order kinetics of the catalytic decomposition of MO and MB were also calculated using the following equation:

$$\ln\left(\frac{C_0}{C}\right) = kt \quad (2)$$

where C_0 and C are the initial and reaction concentrations of MO and MB at time t, respectively [39]. k is the first-order rate constant. The kinetics of the MO degradation using Ag-D/ITO-1, Ag-D/ITO-2 and Ag-D/ITO-3 were 0.03506, 0.04155 and 0.06648 min^{-1}, respectively. The kinetics of the MB degradation using Ag-D/ITO-1, Ag-D/ITO-2 and Ag-D/ITO-3 were 0.03407, 0.03626 and 0.06475 min^{-1}, respectively. The catalytic performance of the Ag-D/ITO-3 towards MO and MB degradation was compared with previous reports in Table 1. The results suggest that the Ag-D coating proposed in this work is a competitive catalyst film for organic pollutant degradation. Noble metal catalysts are known to suffer from poisoning by the reaction products [40]. The reusability of the Ag-D/ITO-3 was examined with regard to consideration in real applications. The coated film is an easy form to use for real applications, since it can be taken out and reapplied for multiple uses. The Ag-D/ITO-3 was taken out after a complete degradation cycle and washed with water and ethanol before the next use. The results show that the Ag-D/ITO-3 retained more than 85% of its original performance at the 5th cycle for both MO and MB degradation. Therefore, the Ag-D coating can be considered an efficient catalyst for the treatment of dye wastewater.

Table 1. Performance comparison of the proposed Ag-D/ITO-3 and other reported catalysts towards the reduction of MO and MB.

Catalyst	MO Rate Constant (min^{-1})	MB Rate Constant (min^{-1})	Reference
RGO/$CoFe_2O_4$	–	0.2651	[41]
$NiCoMnO_4$	–	0.0096	[42]
Biosynthesized Au/Ag	–	0.668	[43]
Au@TiO_2	0.0177	0.0482	[44]
Ag-D/ITO-3	0.06648	0.06475	This work

4. Conclusions

In this work, Ag-D was electrodeposited on an ITO surface for the catalytic degradation of MO and MB in aqueous conditions. The deposition of Ag-D was achieved with the assistance of MWCNTs. The pre-absorption of the Ag ions on the MWCNTs surface provided the Ag nuclei in the initial stage of the electrodeposition. The potential difference between the MWCNT surface and the ITO substrate resulted in the growth of the Ag-D. Due to the porous and supramolecular structure of the Ag-D, a high catalytic performance was recorded when applied for the decomposition of MO and MB dyes.

Supplementary Materials: The following are available online at http://www.mdpi.com/2079-6412/7/12/232/s1, Figure S1: SEM image, UV-Vis spectrum and XRD pattern of MWCNTs.

Acknowledgments: This work has been financially supported by Research Foundation from Hangzhou Dianzi University (KYS205617071) and Zhejiang Province Natural Science Foundation of China (LQ18E010001).

Author Contributions: Li Fu and Zhong Liu conceived and designed the experiments; Li Fu, Kefeng Xie and Huaiwei Zhang performed the experiments; Li Fu and Yuhong Zheng analyzed the data; Weitao Su contributed reagents/materials/analysis tools; Li Fu wrote the paper.

Conflicts of Interest: The authors declare no conflict of interest.

References

1. Zhu, C.; Du, D.; Eychmüller, A.; Lin, Y. Engineering ordered and nonordered porous noble metal nanostructures: Synthesis, assembly, and their applications in electrochemistry. *Chem. Rev.* **2015**, *115*, 8896–8943. [CrossRef] [PubMed]
2. Zhu, C.; Li, H.; Fu, S.; Du, D.; Lin, Y. Highly efficient nonprecious metal catalysts towards oxygen reduction reaction based on three-dimensional porous carbon nanostructures. *Chem. Soc. Rev.* **2016**, *45*, 517–531. [CrossRef] [PubMed]
3. Cho, S.; Jeong, H.; Lee, K.-H. Facile conversion of bulk metal surface to metal oxide single-crystalline nanostructures by microwave irradiation: Formation of pure or Cr-doped hematite nanostructure arrays. *Thin Solid Films* **2017**, *518*, 5110–5114. [CrossRef]
4. Erdem, A.; Meric, B.; Kerman, K.; Dalbasti, T.; Ozsoz, M. Detection of interaction between metal complex indicator and DNA by using electrochemical biosensor. *Electroanalysis* **2015**, *11*, 1372–1376. [CrossRef]
5. Wu, L.-L.; Wang, Z.; Zhao, S.-N.; Meng, X.; Song, X.-Z.; Feng, J.; Song, S.-Y.; Zhang, H.-J. A metal-organic framework/DNA hybrid system as a novel fluorescent biosensor for mercury(II) ion detection. *Chemistry* **2016**, *22*, 477–480. [CrossRef] [PubMed]
6. Llewellyn, D.B.; Adamson, D.; Arndtsen, B.A. A novel example of chiral counteranion induced enantioselective metal catalysis: The importance of ion-pairing in copper-catalyzed olefin aziridination and cyclopropanation. *Org. Lett.* **2015**, *2*, 4165–4168. [CrossRef]
7. Zheng, C.; You, S.-L. Catalytic asymmetric dearomatization by transition-metal catalysis: A method for transformations of aromatic compounds. *Dalton Trans.* **2016**, *25*, 1454–1456. [CrossRef]
8. Shimizu, H. Behavior of metal-induced oxide charge during thermal oxidation in silicon wafers. *J. Electrochem. Soc.* **2016**, *144*, 4335–4340. [CrossRef]
9. Elangovan, D.; Yuzay, I.E.; Selke, S.E.M.; Auras, R. Poly(L-lactic acid) metal organic framework composites: Optical, thermal and mechanical properties. *Polym. Int.* **2015**, *61*, 30–37. [CrossRef]

10. Cong, S.; Yuan, Y.; Chen, Z.; Hou, J.; Yang, M.; Su, Y.; Zhang, Y.; Li, L.; Li, Q.; Geng, F. Noble metal-comparable sers enhancement from semiconducting metal oxides by making oxygen vacancies. *Nat. Commun.* **2015**, *6*, 7800. [CrossRef] [PubMed]
11. Hugall, J.T.; Baumberg, J.J. Demonstrating photoluminescence from au is electronic inelastic light scattering of a plasmonic metal: The origin of sers backgrounds. *Nano Lett.* **2015**, *15*, 2600–2604. [CrossRef] [PubMed]
12. Long, N.V. Engineering of sers substrates based on noble metal nanomaterials for chemical and biomedical applications. *Appl. Spectrosc. Rev.* **2015**, *50*, 499–525.
13. Chen, Y.; Tan, R.; Zhang, Y.; Zhao, G.; Yin, D. Dendritic chiral salen titanium(IV) catalysts enforce the cooperative catalysis of asymmetric sulfoxidation. *Chemcatchem* **2016**, *7*, 4066–4075. [CrossRef]
14. Wang, D.; Deraedt, C.; Ruiz, J.; Astruc, D. Magnetic and dendritic catalysts. *Acc. Chem. Res.* **2015**, *48*, 1871–1880. [CrossRef] [PubMed]
15. Xie, R.; Pan, Y.; Gu, H. Synthesis of Pt dendritic nanocubes with enhanced catalytic properties. *RSC Adv.* **2015**, *5*, 16497–16500. [CrossRef]
16. Vieira, E.G.; Silva, R.O.; Dalbó, A.G.; Frizon, T.E.A.; Filho, N.L.D. Syntheses and catalytic activities of new metallodendritic catalysts. *New J. Chem.* **2016**, *40*, 9403–9414. [CrossRef]
17. Xia, Q.; Jiang, Z.; Wang, J.; Yao, Z. A facile preparation of hierarchical dendritic zero-valent iron for fenton-like degradation of phenol. *Catal. Commun.* **2017**, *100*, 57–61. [CrossRef]
18. Cui, S.; Lu, S.; Xu, W.; Wu, B.; Zhao, N.; He, G.; Hou, X.; Zhang, H. Robust dendritic Ag-Fe_2O_3/Fe surfaces with exquisite catalytic properties. *New J. Chem.* **2016**, *40*, 8897–8904. [CrossRef]
19. Sahoo, P.K.; Thakur, D.; Panigrahy, B.; Bahadur, D. Highly efficient and simultaneous catalytic reduction of multiple dyes using recyclable RGO/Co dendritic nanocomposites as catalyst for the wastewater treatment. *RSC Adv.* **2016**, *6*, 106723–106731. [CrossRef]
20. Rheiner, P.B.; Seebach, D. Dendritic taddols: Synthesis, characterization and use in the catalytic enantioselective addition of Et_2Zn to benzaldehyde. *Chem. A Eur. J.* **2015**, *5*, 3221–3236. [CrossRef]
21. Tajabadi, M.T.; Basirun, W.J.; Lorestani, F.; Zakaria, R.; Baradaran, S.; Amin, Y.M.; Mahmoudian, M.R.; Rezayi, M.; Sookhakian, M. Nitrogen-doped graphene-silver nanodendrites for the non-enzymatic detection of hydrogen peroxide. *Electrochim. Acta* **2015**, *151*, 126–133. [CrossRef]
22. Song, J.; Hou, J.; Tian, L.; Guan, Y.; Zhang, Y.; Zhu, X. Growth of giant silver dendrites on layer-by-layer assembled films. *Polymer* **2015**, *63*, 237–243. [CrossRef]
23. Hu, L.; Liu, Y.J.; Han, Y.; Chen, P.; Zhang, C.; Li, C.; Lu, Z.; Luo, D.; Jiang, S. Graphene oxide-decorated silver dendrites for high-performance surface-enhanced raman scattering applications. *J. Mater. Chem. C* **2017**, *5*, 3908–3915. [CrossRef]
24. Gao, Y.; Xia, B.; Liu, J.; Ding, L.; Li, B.; Zhou, Y. Reversible tuning of the wettability on a silver mesodendritic surface by the formation and disruption of lipid-like bilayers. *Appl. Surf. Sci.* **2015**, *329*, 150–157. [CrossRef]
25. Nersisyan, H.H.; Lee, Y.J.; Joo, S.H.; Han, S.K.; Lee, T.H.; Lee, J.S.; An, Y.S.; Lee, J.H. Iron-assisted electroless deposition reaction for synthesizing copper and silver dendritic structures. *Crystengcomm* **2015**, *17*, 7535–7542. [CrossRef]
26. Guadagnini, L.; Ballarin, B.; Tonelli, D. Dendritic silver nanostructures obtained via one-step electrosynthesis: Effect of nonanesulfonic acid and polyvinylpyrrolidone as additives on the analytical performance for hydrogen peroxide sensing. *J. Nanopart. Res.* **2013**, *15*, 1971. [CrossRef]
27. Fu, L.; Sokiransky, M.M.; Wang, J.; Lai, G.; Yu, A. Development of ag dendrites-reduced graphene oxide composite catalysts via galvanic replacement reaction. *Phys. E Low-dimens. Syst. Nanostruct.* **2016**, *83*, 146–150. [CrossRef]
28. Fu, L.; Lai, G.; Mahon, P.J.; Wang, J.; Zhu, D.; Jia, B.; Malherbe, F.; Yu, A. Carbon nanotube and graphene oxide directed electrochemical synthesis of silver dendrites. *RSC Adv.* **2014**, *4*, 39645–39650. [CrossRef]
29. Fu, L.; Yong, J.; Lai, G.; Tamanna, T.; Notley, S.; Yu, A. Nanocomposite coating of multilayered carbon nanotube–titania. *Mater. Manuf. Process.* **2014**, *29*, 1030–1036. [CrossRef]
30. Witten, T.A., Jr.; Sander, L.M. Diffusion-limited aggregation, a kinetic critical phenomenon. *Phys. Rev. Lett.* **1981**, *47*, 1400–1403. [CrossRef]
31. Ben-Jacob, E.; Garik, P. The formation of patterns in non-equilibrium growth. *Nature* **1990**, *343*, 523–530. [CrossRef]

32. Huang, Y.F.; Zhang, M.; Zhao, L.B.; Feng, J.M.; Wu, D.Y.; Ren, B.; Tian, Z.Q. Activation of oxygen on gold and silver nanoparticles assisted by surface plasmon resonances. *Angew. Chem. Int. Ed.* **2014**, *53*, 2353–2357. [CrossRef] [PubMed]
33. Kaniyankandy, S.; Nuwad, J.; Thinaharan, C.; Dey, G.K.; Pillai, C.G.S. Electrodeposition of silver nanodendrites. *Nanotechnology* **2007**, *18*, 125610. [CrossRef]
34. Rashid, M.H.; Mandal, T.K. Synthesis and catalytic application of nanostructured silver dendrites. *J. Phys. Chem. C* **2007**, *111*, 16750–16760. [CrossRef]
35. Wang, X.; Itoh, H.; Naka, K.; Chujo, Y. Tetrathiafulvalene-assisted formation of silver dendritic nanostructures in acetonitrile. *Langmuir* **2003**, *19*, 6242–6246. [CrossRef]
36. Vidhu, V.K.; Philip, D. Catalytic degradation of organic dyes using biosynthesized silver nanoparticles. *Micron* **2014**, *56*, 54–62. [CrossRef] [PubMed]
37. Frelink, T.; Visscher, W.; Van Veen, J. Particle size effect of carbon-supported platinum catalysts for the electrooxidation of methanol. *J. Electroanal. Chem.* **1995**, *382*, 65–72. [CrossRef]
38. Zhou, W.; Liu, Q.; Zhu, Z.; Zhang, J. Preparation and properties of vanadium-doped TiO_2 photocatalysts. *J. Phys. D Appl. Phys.* **2010**, *43*, 035301. [CrossRef]
39. Houas, A.; Lachheb, H.; Ksibi, M.; Elaloui, E.; Guillard, C.; Herrmann, J.-M. Photocatalytic degradation pathway of methylene blue in water. *Appl. Ctatl. B Environ.* **2001**, *31*, 145–157. [CrossRef]
40. Ji, Z.; Shen, X.; Yang, J.; Zhu, G.; Chen, K. A novel reduced graphene oxide/Ag/CeO_2 ternary nanocomposite: Green synthesis and catalytic properties. *Appl. Ctatl. B Environ.* **2014**, *144*, 454–461. [CrossRef]
41. Wu, Q.; Zhang, H.; Zhou, L.; Bao, C.; Zhu, H.; Zhang, Y. Synthesis and application of RGO/$CoFe_2O_4$ composite for catalytic degradation of methylene blue on heterogeneous fenton-like oxidation. *J. Taiwan Inst. Chem. Eng.* **2016**, *67*, 484–494. [CrossRef]
42. Li, K.; Luo, X.; Lin, X.; Qi, F.; Wu, P. Novel nicomno4 thermocatalyst for low-temperature catalytic degradation of methylene blue. *J. Mol. Catal. A Chem.* **2014**, *383–384*, 1–9. [CrossRef]
43. Suvith, V.S.; Philip, D. Catalytic degradation of methylene blue using biosynthesized gold and silver nanoparticles. *Spectrochim. Acta Part A Mol. Biomol. Spectrosc.* **2014**, *118*, 526–532. [CrossRef] [PubMed]
44. Khan, M.M.; Lee, J.; Cho, M.H. Au@TiO_2 nanocomposites for the catalytic degradation of methyl orange and methylene blue: An electron relay effect. *J. Ind. Eng. Chem.* **2014**, *20*, 1584–1590. [CrossRef]